

# Reversal of the Charge Transfer between Host and Dopant Atoms in Semiconductor Nanocrystals

Torbjörn Blomquist and George Kirczenow<sup>y</sup>

Department of Physics, Simon Fraser University, Burnaby, British Columbia, Canada V5A 1S6  
(Dated: March 22, 2024)

We present *ab initio* density functional calculations that show P (Al) dopant atoms in small hydrogen-terminated Si crystals to be negatively (positively) charged. These signs of the dopant charges are reversed relative to the same dopants in bulk Si. We predict this novel reversal of the dopant charge (and electronic character of the doping) to occur at crystal sizes of order 100 Si atoms. We explain it as a result of competition between fundamental principles governing charge transfer in bulk semiconductors and molecules and predict it to occur in nanocrystals of most semiconductors.

PACS numbers: 73.22.-f

Introducing appropriate impurity atoms (known as "dopants") into a semiconductor can dramatically affect electrical conduction in the material and is key to the operation of modern electronic devices.[1] The dopant atoms modify the conductivity of the semiconductor by supplying it with additional free electrons or holes that can carry an electric current. If an impurity atom having one more electron than an atom of the semiconductor host replaces a host atom, in many cases the extra electron is very weakly bound to the impurity atom in the solid state environment.[2] Thus at room temperature the shallow impurity loses (donates) the extra electron to the semiconductor and the impurity atom becomes positively charged. Conversely an impurity atom with one fewer electron than the host accepts an electron from the host, becomes negatively charged, and a positively charged free hole appears in the semiconductor. This qualitative picture of charge transfer between semiconductor host and shallow dopant is well established for bulk semiconductor materials and is fundamental to our understanding of the properties of semiconductor devices. Recent experimental and theoretical work [3, 4, 5, 6, 7, 8, 9, 10] has shown that it also holds for a variety of doped semiconductor nanoparticles.

Charge transfer also plays an important role in the chemistry of molecular systems [11], however, the basic principles that apply in this case are different: Atoms are classified according to their electronegativity which is defined so that an atom with a larger electronegativity will attract (negative) electronic charge from an atom with smaller electronegativity. Atoms with nearly filled valence orbitals have large electronegativities because filled orbitals are energetically stable. Conversely atoms with nearly empty valence orbitals have low electronegativities. Simple semiconductors consisting of atoms from group IV of the periodic table have precisely half-filled valence orbitals. A group V atom has one more valence electron and since its valence orbitals are closer to being filled it has a larger electronegativity. Therefore, according to this picture, a dopant atom with one more electron than the host semiconductor should attract charge from

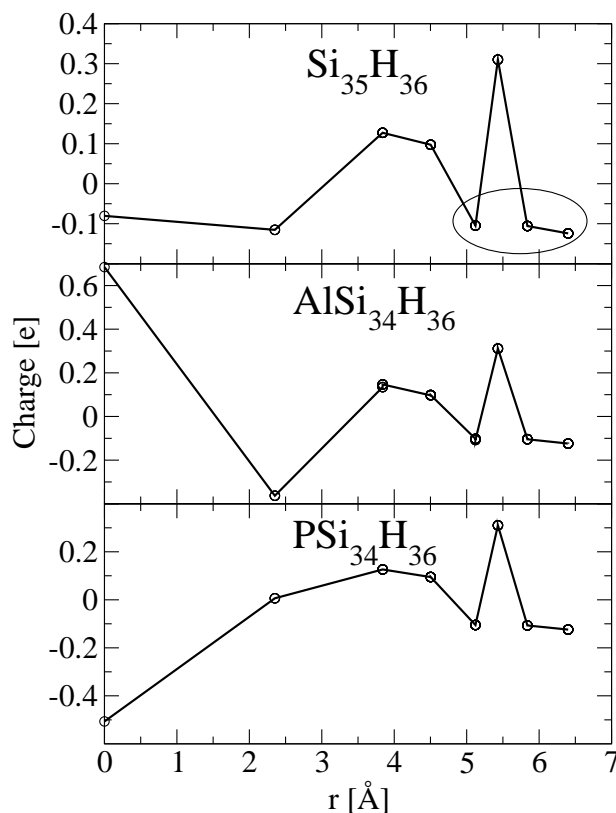


FIG. 1: On site natural population [19] charge as function of the site radial coordinate for  $\text{Si}_{35}\text{H}_{36}$ . Undoped crystallite in top graph. The ellipse in the top graph shows which atoms are hydrogen. The central atom (at  $r = 0$ ) has been replaced with aluminum (acceptor in bulk Si) in center graph and with phosphorus (donor in bulk Si) in bottom graph.

the surrounding host atoms and carry a negative charge. Similarly a group III dopant atom with one fewer electron than the host would be positive. Clearly this reasoning based on considerations of molecular chemistry predicts charge transfer between dopant and host opposite in sign to that found in the solid state semiconductor systems discussed above. This raises the intriguing, and until now unrecognized, possibility that charge transfer in doped

semiconductor nanocrystals with dimensions approaching the molecular scale might differ fundamentally from that in macroscopic semiconductors, with profound implications for the electronic properties of nanoscale semiconductor devices. Here we show theoretically that this is in fact the case and explore the crossover between the conventional (macroscopic) and novel nanoscopic/quasimolecular (reversed charge transfer) doping regimes.

Representative results of our *ab initio* density functional calculations [12] of the charge distributions in some small H-terminated Si crystals doped with P and Al are shown in Fig. 1. Since a P (Al) atom has one more (less) valence electron than Si, in bulk Si the shallow dopant P (Al) is an electron donor (acceptor) and the impurity site is positively (negatively) charged. In Fig. 1, however, the reverse is true. Thus our results for these Si nanocrystals clearly demonstrate the existence of the quasimolecular regime that we have proposed above, where charge transfer is governed by electronegativity considerations rather than by the standard theory of doping in bulk semiconductors.

*Ab initio* quantum chemistry calculations such as those that yielded the results of Fig. 1 cannot at present be made for much larger crystallites due to practical limitations of computers. We have therefore developed a Poisson-Schrodinger (PS) model for silicon based on a nonorthogonal tight-binding (TB) model in order to explore the crossover from the quasimolecular regime to crystals large enough that standard semiconductor theory should be appropriate. We have also examined how energy gaps and dopant levels evolve with the size of the Si crystallite.

We have based our TB model on that of Bernstein et al. [13] which reproduces the band structure of silicon very well, and gives reasonable values for electron and hole masses, see table I. The on-site potentials in the Bernstein model are however functions of the local density of atoms but differences in on-site potentials are explicitly given by the PS scheme, so we have used Bernstein's values for bulk Si as a starting point for the PS scheme. On-site potentials for hydrogen and hopping integrals for Si-H have been fitted to reproduce charge distributions obtained from *ab initio* density functional calculations. [12] We have used the same overlap and hopping integrals for Al-Si and P-Si as for Si-Si. The on-site parameters for Al and P have been fitted to yield the correct sign of the charge on the impurity site for small crystals and realistic values for dopant energy levels for large ones. The on-site electron repulsion energies for Al, Si and P are based on valence orbital ionization energies taken from table D 4 of Ref. 14; equation (D 6) in Ref. 14 is used for H. We have ensured that our model reproduces the on-site energies and band structure of the Bernstein model for bulk Si.

TABLE I: Some properties of the TB model, [13] experimental values are given in parenthesis. [20]

Position of conduction band minimum	87.7%	X	(85%)
Band gap	1.01 eV		(1.12)
Light hole mass	0.26 $m_e$		(0.15)
Heavy hole mass	0.31 $m_e$		(0.54)
Longitudinal electron mass	0.55 $m_e$		(0.92)
Transverse electron mass	0.15 $m_e$		(0.19)

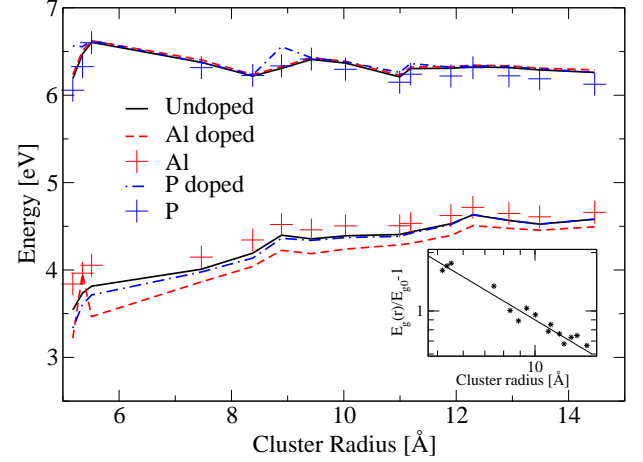


FIG. 2: (Color online) The energies of the valence and conduction bands of the crystallites, with and without dopants, plotted as functions of crystallite radius. The energies of the dopant states are also shown. The inset shows the band gap plotted as  $f(r) = E_g(r)/E_{g0} - 1$  on a log-log-scale for comparison with papers 15, 16. A fit,  $f(r) = 9.0r^{-1.0}$  is also shown.

The energy on site  $i$  includes the electrostatic term

$$V_i = \frac{1}{\epsilon_r} \sum_{j \neq i} \frac{q_j}{r_{ij}} + \int_S \frac{\sigma(r)}{r_{ij}} dr; \quad (1)$$

where  $\epsilon_r$  is the relative dielectric constant due to core polarization (core electrons are not included in the TB model) in Si,  $q_j$  is the net charge on site  $j$ ,  $r_i$  is the position of site  $i$ ,  $S$  is the surface of the structure and  $\sigma(r)$  is the surface polarization charge, due to the core polarization. We have chosen the value  $\epsilon_r = 6.5$  so that the model reproduces the correct total dielectric constant of 11.8 for infinite Si slabs, taking into account polarization of both the valence and core electrons. The electrostatic equation is solved self-consistently together with the Schrodinger equation  $H = ES$  for the nonorthogonal TB model. Here  $S$  are overlap integrals. The charge on each site is calculated using Mulliken population analysis. [14]

We have applied the present model to calculate the ground state properties of a number of silicon nanocrystals ranging in size from  $\text{Si}_{29}\text{H}_{36}$  to  $\text{Si}_{633}\text{H}_{300}$ , with and without dopants. All of them are approximately spherical, have tetrahedral symmetry, and are hydrogen

TABLE II: Band gaps for undoped and doped crystallites. Dopant levels for the doped nanocrystals.

Crystallite	gap (eV)	P gap (eV)	Al gap (eV)	P level (meV)	Al level (meV)
Si <sub>29</sub> H <sub>36</sub>	2.64567	3.22941	3.01460	507.92	618.78
Si <sub>32</sub> H <sub>36</sub>	2.73479	2.95265	2.54536	229.18	2.46
Si <sub>35</sub> H <sub>36</sub>	2.79060	2.91065	3.15534	24.37	587.29
Si <sub>77</sub> H <sub>76</sub>	2.36659	2.39807	2.53979	60.15	284.22
Si <sub>123</sub> H <sub>100</sub>	2.02584	2.09530	2.19588	5.69	303.12
Si <sub>147</sub> H <sub>100</sub>	1.90885	2.19233	2.09923	219.87	295.63
Si <sub>175</sub> H <sub>116</sub>	2.05314	2.08903	2.24444	14.17	271.98
Si <sub>211</sub> H <sub>140</sub>	1.97595	2.00978	2.14665	84.48	265.58
Si <sub>278</sub> H <sub>172</sub>	1.80325	1.87565	1.93952	111.71	217.66
Si <sub>293</sub> H <sub>172</sub>	1.86942	1.94209	2.01869	122.92	229.42
Si <sub>353</sub> H <sub>196</sub>	1.77987	1.80023	1.93001	100.28	226.42
Si <sub>389</sub> H <sub>196</sub>	1.69254	1.70375	1.83677	22.85	209.68
Si <sub>453</sub> H <sub>228</sub>	1.74891	1.75739	1.85943	105.10	169.72
Si <sub>513</sub> H <sub>252</sub>	1.76443	1.77445	1.85331	111.99	152.69
Si <sub>633</sub> H <sub>300</sub>	1.68004	1.67888	1.79626	135.37	166.78

terminated to obtain a clean energy gap for the undoped nanocrystals.[15]

Figure 2 and Table II show how the energies of the valence band, conduction band and dopant levels change with nanocrystal size. The conduction band energy varies little with nanocrystal size and dopant species. The valence band moves up narrowing the band gap to 1.7 eV for Si<sub>633</sub>H<sub>300</sub> from 2.7 eV for Si<sub>29</sub>H<sub>36</sub>. Doping widens the band gap somewhat, but this effect is most significant for the smallest crystals. The band gap can be fitted to a function  $E_g(d) = E_{g0} - 1/r^b$ , where  $r = 1.68456N^{1/3}$  is the radius of the crystallite,  $N$  is the number of Si atoms,  $E_{g0}$  is the band gap in the bulk and,  $A$  and  $b$  are fitting parameters. We find that  $A = 9.0$  and  $b = 1.0$ ; see fitted line in inset of Fig. 2. Liu et al.[15] and Zunger et al.[16] report  $b = 1.37$  in models without Coulomb interactions. Effective mass theory (particle in a box) predicts an  $r^{-2}$  scaling. Our result, however, agrees very well with density functional theory calculations [4, 17, 18].

There has been interest in how the system size affects the dopant levels and there has been a number of studies using different methods, for example effective mass theory,[5, 6, 7] TB,[8] PRDDO [9] and DFT.[10] Our results are consistent with this previous work. We define the dopant level as the energy difference between the partially filled dopant state and its nearest neighbor state. The Al dopant levels in the nanocrystals, see Table II, vary quite smoothly with crystal size (AlSi<sub>31</sub>H<sub>36</sub> is an exception), down to about three times the bulk value (57 meV) for AlSi<sub>632</sub>H<sub>300</sub>. The P dopant levels on the other hand vary a lot from cluster to cluster, but also reach about three times the bulk value (45 meV) for our

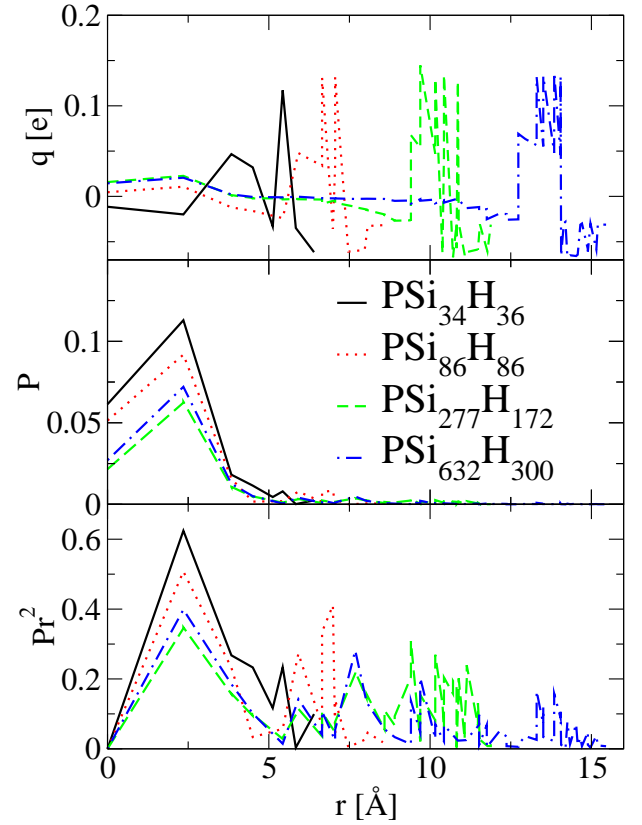


FIG. 3: (Color online) Top graph, total Mulliken charge on each site as function of radial coordinate for four different P-doped clusters. Center graph, Mulliken probability distribution for the donor state. Bottom graph, probability distribution multiplied by radial coordinate squared to approximate probability of finding the electron at a certain radius.

largest crystallite. We attribute this difference between the acceptor and donor states to the fact that the electron states have a larger probability on the surface sites, making donor states much more sensitive to the surface than acceptor states which typically are more localized to the interior of the cluster; see the bottom graphs of Figs. 3 and 4. The strong variations for the donor state levels suggest that it would be difficult to engineer the properties of a small n-doped cluster without atomic control in the manufacturing. It is also relevant in this regard that the bands in these small structures are made up from discrete energy levels and even for our largest crystallites, these levels have an energy spacing of 5–50 meV.

The charge on the impurity site ( $r = 0$ ) for the phosphorus doped crystallites in Fig. 3 exhibits a crossover from negative to positive when going from small to large nanocrystals. This crossover between the quasi-molecular behavior and the bulk semiconductor behavior occurs between PSi<sub>34</sub>H<sub>36</sub> and PSi<sub>86</sub>H<sub>86</sub>. For the aluminum doped crystallites (Fig. 4) we find a crossover from a positive to a negative impurity site between AlSi<sub>22</sub>H<sub>100</sub> and AlSi<sub>46</sub>H<sub>100</sub>. The precise crossover

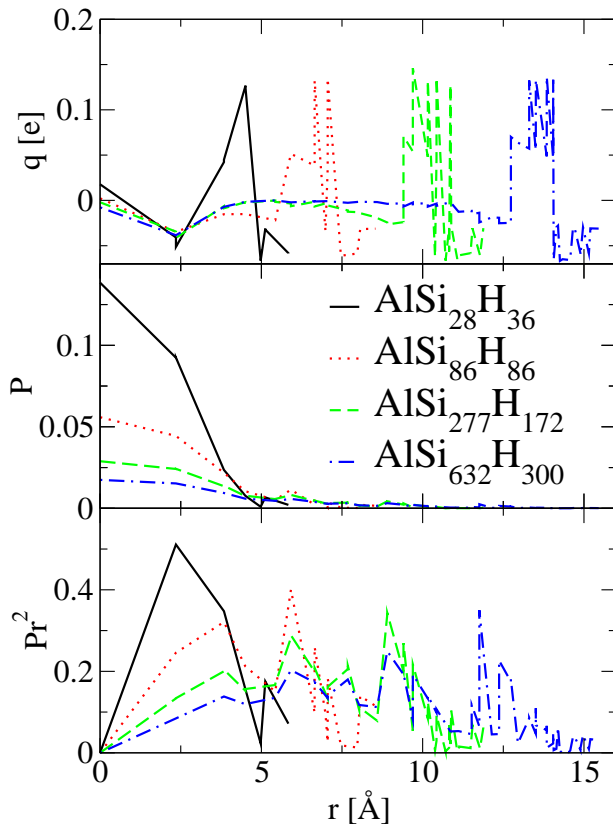


FIG. 4: (Color online) Top graph, total Mulliken charge on each site as function of radial coordinate for four different Al-doped clusters. Center graph, Mulliken probability distribution for the acceptor state. Bottom graph, probability distribution multiplied by radial coordinate squared to approximate probability of finding the hole at a certain radius.

points are sensitive to the parameters of the model and this result should be regarded as the first (order of magnitude) estimate. The charges on the impurity site in Figs. 3 and 4 are consistently somewhat smaller in magnitude than in Fig. 1; we attribute this difference to the fact that Mulliken population analysis (Figs. 3 and 4), tends to smear charge between overlapping orbitals on neighboring atoms more than do natural orbital calculations (Fig. 1).

In conclusion: The Poisson-Schrodinger model we have developed has allowed us to explore the crossover from a novel regime in semiconductor nanocrystals in which the molecular view of charge transfer between atoms holds true to a regime where macroscopic solid state semiconductor theory prevails. The crossover is signaled by a striking reversal of the sign of the charge transfer between the host semiconductor and dopant atom that has not been anticipated in previous experimental or theoretical work. We predict that it should occur at nanocrystal sizes of order 100 Si atoms. Since very basic principles of solid state semiconductor physics and molecu-

lar chemistry are the underlying reasons for the charge reversal, we predict it to be a general phenomenon occurring for a wide variety of nanoscopic semiconductors and dopants. For Si nanocrystals we also find an energy gap widening that scales as  $r^{-1.0}$  consistent with density functional theory calculations.[4, 17, 18] We predict the dopant energy levels for Al in Si nanocrystals to vary quite smoothly with cluster size while donor levels should vary widely from crystallite to crystallite, making it difficult to engineer properties of P-doped Si nanocrystals without atomic control in manufacturing.

This work was supported by NSERC and the Canadian Institute for Advanced Research.

Electronic address: tobmqui@sfu.ca

<sup>y</sup> Electronic address: kirczeno@sfu.ca

- [1] C. Kittel, Introduction to solid state physics (Wiley, New York, 1996), 7th ed.
- [2] W. Kohn, Phys. Rev. 105, 509 (1957).
- [3] A. M. Inura, M. Fujii, S. Hayashi, D. Kovalev and F. Koch, Phys. Rev. B 62 12625 (2000).
- [4] D. V. Melnikov and J. R. Chelikowsky, Phys. Rev. Lett. 92 046802 (2004).
- [5] R. K. Pandey, M. K. Harbola and V. V. Singh, cond-mat/0308029 (2003).
- [6] J.-L. Zhu, J.-J. Xiong and B.-L. Gu, Phys. Rev. B 41, 6001 (1990).
- [7] B. Stebe, E. Assaid, F. Du Jardin, and S. Le Go, Phys. Rev. B 54, 17785 (1996).
- [8] G. T. Enevoll and Y.-C. Chang, Phys. Rev. B 40, 9683 (1989).
- [9] S. E. Streicher, Phys. Rev. B 37 858 (1988).
- [10] M. Lannoo, C. Delerue, and G. Allan, Phys. Rev. Lett. 74, 3415 (1995).
- [11] H. S. Stoker, Introduction to Chemical Principles (Macmillan, New York, 1993), 4th ed.
- [12] We employed the gaussian 98 numerical implementation of density functional theory with the 6-31G(d) basis set and the B3LYP exchange-correlation energy functional.
- [13] N. Bernstein, M. J. Mehl, D. A. Papaconstantopoulos, N. I. Papanicolaou, M. Z. Bazant, and E. Kaxiras, Phys. Rev. B 62, 4477 (2000), *ibid.* 65, 249902 (E) (2002).
- [14] S. P. McGlynn, L. G. Vanquickenborne, M. K. Inoshita, D. G. Carroll, Introduction to Applied Quantum Chemistry (Holt, Rinehart and Winston, Inc, New York, 1972)
- [15] L. Liu, C. S. Jayanthi, S.-Y. Wu, cond-mat/0012217 (2003).
- [16] A. Zunger, L.-W. Wang, Appl. Surf. Sci. 102, 350 (1996).
- [17] B. Delley and E. F. Steigmeyer, Phys. Rev. B 47, 1397 (1993); Appl. Phys. Lett. 67, 2370 (1995).
- [18] S. Ogut and J. R. Chelikowsky, and S. G. Louie, Phys. Rev. Lett. 79, 1770 (1997).
- [19] A. E. Reed, L. A. Curtiss and F. Weinhold, Chem. Rev. 88, 899 (1988).
- [20] O. Madelung, Semiconductors Group IV Elements and III-V Compounds (Springer-Verlag, Berlin, 1991)